Sea Ice Surface Temperature Product From MODIS

Dorothy K. Hall, *Senior Member, IEEE*, Jeffrey R. Key, Kimberly A. Casey, George A. Riggs, and Donald J. Cavalieri

***Abstract*—Global sea ice products are produced from the Earth Observing System (EOS) Moderate Resolution Imaging Spectroradiometer (MODIS) onboard both the Terra and Aqua satellites. Daily sea ice extent and ice surface temperature (IST) products are available at 1- and 4-km resolution. Validation activities during the "cold period" (when meltwater is generally not present) in the Northern Hemisphere, defined here as October through May, have been undertaken to assess the accuracy of the 1-km resolution MODIS IST algorithm and product. Validation was also done at the South Pole station in Antarctica. In the Arctic Ocean, near-surface air temperatures from the National Oceanic and Atmospheric Administration (NOAA) National Ocean Service (NOS) Center for Operational Oceanographic Products and Services (CO-OPS) Alaska tide stations and from drifting buoys from the North Pole Environmental Observatory (NPEO) buoy program were compared with MODIS-derived ISTs. Using the standard MODIS sea ice product, which utilizes the MODIS cloud mask, results show a bias (mean error) of −2.1 K and a root mean square (RMS) error of 3.7 K. The negative bias means that the satellite retrieval is less than the air temperature. With the bias removed, the RMS error is 3.0 K. When additional visual cloud screening is performed to eliminate MODIS pixels thought to be contaminated by fog, results improved, with a subset of the larger dataset showing a bias of −0.9 K and an RMS error of 1.6 K. Uncertainties would be reduced in the Arctic Ocean dataset if the skin temperature of the sea ice were reported instead of the near-surface air temperatures. With the bias removed, the RMS error for the Arctic Ocean dataset is 1.3 K. Results from the South Pole station in Antarctica show that under clear skies as determined using lidar measurements, the MODIS ISTs are also very close to those of the near-surface air temperatures with a bias of −1.2 K and an RMS error of 1.7 K. With the bias removed, the RMS error for the South Pole dataset is 1.2 K. Thus, the accuracy (RMS error) of the IST measurement is 1.2–1.3 K. It is not possible to obtain an accurate IST from MODIS in the presence of even very thin clouds or fog, and this is the main limitation of the MODIS ice surface temperature product. MODIS sea ice products may be ordered from the National Snow and Ice Data Center in Boulder, CO.**

***Index Terms*—Advanced Microwave Scanning Radiometer-EOS (AMSR-E), ice-surface temperature, Moderate-Resolution Imaging Spectroradiometer (MODIS), sea ice.**

Manuscript received July 14, 2003; revised January 3, 2004. This work was supported by the National Aeronautics and Space Administration's Earth Science Enterprise under the EOS Project. The work of J. R. Key was supported by the National Oceanic and Atmospheric Administration and by the Integrated Program Office.

D. K. Hall is with the NASA Goddard Space Flight Center, Greenbelt, MD 20771 USA (e-mail: dorothy.k.hall@nasa.gov).

J. R. Key is with the NOAA National Environmental Satellite, Data and Information Service, Madison, WI 53706 USA.

K. A. Casey and G. A. Riggs are with the Science Systems and Applications, Inc., Lanham, MD 20706 USA.

D. J. Cavalieri is with the NASA Goddard Space Flight Center, Greenbelt, MD 20771 USA.

Digital Object Identifier 10.1109/TGRS.2004.825587

I. Introduction

THE PRESENCE of sea ice influences the temperature and circulation patterns of both the atmosphere and the oceans. Sea ice reduces the amount of solar radiation absorbed at the ocean surface and, with the overlying snow cover, serves as an insulator, restricting exchanges of heat, momentum, and chemical constituents between the atmosphere and the ocean. Its large area coverage, 5% of the ocean surface, makes the sea ice cover a key parameter in the earth's energy balance. Ice surface temperature (IST) controls snow metamorphosis and melt, the rate of sea ice growth, and air–sea heat exchange and is an important parameter in large-scale modeling.

The importance of obtaining climate data records of sea ice in the form of high-resolution validated global sea ice maps is highlighted by recent studies showing decade-scale changes in the global sea ice extent. Several authors have shown that the extent of sea ice in the Arctic has decreased since 1979 by ∼3% per decade [1]–[3], while in the Southern Ocean the extent of sea ice increased ∼1% per decade from 1979 to 1998 [4]. More recently, from an analysis of a 30-year sea ice record, the rate of decrease in Arctic sea ice was found to be 20% greater since 1979 than since 1971, while the overall trend in the Antarctic was found to be negative over the 30-year period as a result of anomalously large ice extents in the early 1970s [5]. Most of these studies have used spaceborne coarse-resolution (∼25 km) passive microwave instruments to monitor the sea ice. Additionally, a warming trend in the Arctic has been measured using satellite-derived thermal-infrared data on surface temperatures [6].

Two classes of sensors—microwave and multispectral radiometers—are typically used for global mapping of sea ice extent, concentration, type, and temperature. The ability of microwave instruments, both passive and active, to collect data through cloud cover and polar darkness makes them well suited to global monitoring of sea ice extent and dynamics. Passive-microwave data can also provide a measure of near-surface ice temperature [7]–[12] though the location, at some depth within the snow/ice volume, that the temperature represents varies with ice type. However, microwave instruments cannot collect data on IST or sea ice albedo, and they have a relatively coarse spatial resolution that limits their utility for detailed studies of sea ice dynamics. In contrast, visible, near-infrared, and/or infrared sensors can provide detail on the ice extent and concentration during clear-sky conditions as well as on snow/ice albedo and IST.

The Moderate-Resolution Imaging Spectroradiometer (MODIS), flown on both the Terra and Aqua satellites (launched in December 1999 and May 2002, respectively), is useful for determination of sea ice extent, albedo, movement, type, and concentration at resolutions ranging from 0.25–1 km,

and IST can be determined at 1-km resolution. Daily extent and IST map products are produced at the MODIS Data Processing System (MODAPS) facility at the Goddard Space Flight Center, Greenbelt (GSFC), MD, using MODIS data at 1-km resolution. The MODIS sea ice products were developed at GSFC and are archived and distributed by the National Snow and Ice Data Center (NSIDC) in Boulder, CO.

The purpose of this paper is to describe the algorithm used to create the MODIS IST maps, show examples of the IST products, and provide validation information for the algorithm and products during the cold period in the Arctic Basin and at the South Pole.

II. Background

Global year-round records of ice-covered Arctic and Antarctic seas were acquired from several satellite passive-microwave radiometers beginning with the Nimbus-5 Electrically Scanning Microwave Radiometer (1972–1977), followed by the Nimbus-7 Scanning Multichannel Microwave Radiometer (1978–1987), and then by the series of Defense Meteorological Satellite Program Special Sensor Microwave/Imagers (SSM/I) (1987 to the present). The acquisition of microwave radiances from these sensors has allowed the production of hemispheric sea ice concentration maps and global time series of sea ice extent and area [1], [8], [11], [12]. Sea ice maps derived from visible, near-infrared, and infrared sensors have also been available from the National Oceanic and Atmospheric Administration (NOAA) National Ice Center (NIC) since 1972 [13] and are currently available from MODIS (from February 24, 2000, to the present).

Measurement of sea ice surface temperature is possible with optical and thermal-infrared sensors such as the Temperature Humidity Infrared Radiometer (THIR), Advanced Very High Resolution Radiometer (AVHRR), Landsat Thematic Mapper (TM), Enhanced Thematic Mapper Plus (ETM+) [14]–[19], and MODIS. Comparisons of AVHRR-derived ice surface temperature with measurements during the Surface Heat Budget of the Arctic (SHEBA) experiment [20] and other field experiments show that the clear-sky IST can be estimated with an accuracy (root mean square (RMS) error) of 0.3–3.0 K [17], [19], [21], [22].

An important heritage of the MODIS IST products is the AVHRR Polar Pathfinder dataset. The AVHRR Polar Pathfinder Twice-Daily 5 km EASE-Grid Composites (http://www.nsidc.org/data/nsidc-0066.html) is a collection of products for both poles consisting of twice-daily gridded and calibrated satellite channel data and derived parameters including five AVHRR channels, clear-sky surface broadband albedo and skin temperature, solar-zenith angle, satellite-elevation angle, sun-satellite relative azimuth angle, surface type mask, cloud mask, and Coordinated Universal Time (UTC) of acquisition [23]–[25], and 25-km resolution data, derived from the 5-km data, are also available. AVHRR Polar Pathfinder data extend poleward from 48.4° north and 53.2° south latitudes and provide data from July 1981 through August 1998.

For the retrieval of clear-sky IST, a split-window technique is typically used, where "split-window" refers to brightness–temperature differences in the 11–12-μm atmospheric window. This technique allows for the correction of atmospheric effects primarily due to water vapor. First employed to determine sea surface temperature [26], the technique was subsequently used to determine IST in the Arctic with the AVHRR on NOAA polar-orbiting satellites [16]. This work was later refined and expanded to include ice surfaces in both polar regions and a broader range of atmospheric conditions. Several other investigators have employed variations of the split-window method for estimation of IST in the polar regions using the AVHRR and other instruments (e.g., [17] and [27]–[29]).

Sea ice skin temperature from AVHRR was used to "calibrate" the SSM/I data to estimate surface temperature and cloud cover in the Arctic [29]. AVHRR-derived temperatures for clear-sky conditions were used to derive effective emissivities for first-year and multiyear sea ice. Given these emissivities, and parameters derived from the SSM/I, physical temperatures of the sea ice or snow surface may be calculated that are relatively independent of cloud conditions, though absolute accuracy of the remotely derived temperatures could not be determined [29].

Long-term emissivity variations from SSM/I data were used to reconstruct the physical temperature trend from brightness temperature data [9]. The temperature cycle tracks air temperature with little lag [9], [30].

III. MODIS Sea Ice Algorithms

MODIS is an imaging spectroradiometer (http://modis.gsfc.nasa.gov) that provides imagery of the earth's surface and clouds in 36 discrete, narrow spectral bands from approximately 0.4–14.0 μm at resolutions ranging from 0.25–1 km at nadir [31]. Global vegetation and land cover, global land-surface change, vegetation properties, surface albedo, land and ice surface temperature, and snow and ice cover [32] products from MODIS are available on a daily or regular basis [33].

MODIS sea ice data products are produced as a sequence of products, beginning with a swath (scene) at a nominal pixel spatial resolution of 1 km and a nominal swath coverage of 2330 km (cross track) $\times$ 2030 km (along track) (about 5 min of satellite travel), and ending with a monthly global map product (Table I). Automated selection of the most favorable observation from all the swaths acquired during a day generates a daily gridded sea ice product. A daily global product of sea ice extent and IST at $\sim$4-km resolution in the Equal-Area Scalable Earth Grid (EASE-Grid) projection [34] (http://nsidc.org/data/ease/) has been developed and is being tested. Eight-day composite sea ice products, covering the north and south polar regions separately (Fig. 1), and monthly global sea ice products will become available in 2004.

Because the swath algorithm will often map clouds as sea ice, we use the MODIS cloud mask product to mask the clouds. If the cloud mask fails to map a cloud, then it will be mapped by the sea ice algorithm as sea ice. To avoid such errors of commission, the algorithm that produces the eight-day composite maps requires that sea ice be visible two days in a row in order to be mapped as sea ice.

TABLE I
DETAILED DATA PRODUCT DESCRIPTION OF MODIS SEA ICE DATA PRODUCTS.
*FUTURE ENHANCEMENT OR PRODUCT (TO BE IMPLEMENTED IN 2004)

Long Name	Earth Science Data Type (ESDT)	Spatial Resolution
MODIS/Terra Sea Ice Extent 5-Min L2 Swath 1km	MOD29	1-km resolution, swath of MODIS data
MODIS/Terra Sea Ice Extent Daily L3 Global EASE-Grid Day	MOD29P1D	1-km resolution, projected, gridded tile data
MODIS/Terra Sea Ice Extent Daily L3 Global EASE-Grid Night	MOD29P1N	1-km resolution, projected, gridded tile data
MODIS/Terra Sea Ice Extent and Ice Surface Temperature Daily L3 Global 4km EASE-Grid Day *	MOD29E1D	4-km resolution, global, gridded
MODIS/Terra Ice Surface Temperature Daily L3 Global 4km EASE-Grid Night *	MOD29E1N	4-km resolution, global, gridded
MODIS/Terra Sea Ice Extent and Ice Surface Temperature 8-Day L3 Global EASE-Grid Day *	MOD29E2D	4-km resolution, global, gridded
MODIS/Terra Ice Surface Temperature 8-Day L3 Global EASE-Grid Night*	MOD29E2N	4-km resolution, global, gridded
MODIS/Terra Sea Ice Extent and Ice Surface Temperature Monthly L3Global 4km EASE-Grid Day*	MOD29EMD	4-km resolution, global, gridded
MODIS/Terra Ice Surface Temperature Monthly L3Global 4km EASE-Grid Night *	MOD29EMN	4-km resolution, global, gridded
MODIS/Aqua Sea Ice Extent 5-Min L2 Swath 1km	MYD29	1-km resolution, swath of MODIS data
MODIS/Aqua Sea Ice Extent Daily L3 Global EASE-Grid Day*	MYD29P1D	1-km resolution, projected, gridded tile data
MODIS/Aqua Sea Ice Extent Daily L3 Global EASE-Grid Night*	MYD29P1N	1-km resolution, projected, gridded tile data
MODIS/Aqua Sea Ice Extent and Ice Surface Temperature Daily L3 Global 4km EASE-Grid Day*	MYD29E1D	4-km resolution, global, gridded
MODIS/Aqua Ice Surface Temperature Daily L3 Global 4km EASE-Grid Night *	MYD29E1N	4-km resolution, global, gridded
MODIS/Aqua Sea Ice Extent and Ice Surface Temperature 8-Day L3 Global EASE-Grid Day *	MYD29E2D	4-km resolution, global, gridded
MODIS/Aqua Ice Surface Temperature 8-Day L3 Global EASE-Grid Night*	MYD29E2N	4-km resolution, global, gridded
MODIS/Aqua Sea Ice Monthly Global EASE-Grid *	MYD29EMD	4-km resolution, global, gridded

Algorithms for deriving the sea ice map products from MODIS are similar for both the Terra and the Aqua MODIS instruments and are used to generate maps of sea ice extent as determined by reflectance and IST and a combined map product that provides sea ice extent by reflectance and IST [35], [36]. The products are produced globally at both 1-km and ~4-km spatial resolution. During daylight hours, sea ice map products are derived from reflectances and from IST, while at nighttime, only the IST maps are produced (Table I). MODIS sea ice products are generated automatically using MODIS sensor-radiance data [37], a geolocation product [38], and the MODIS cloud mask product [35], [39]. In addition to sea ice extent and IST, quality assurance, latitude and longitude, and other information are also included with the data products.

Fig. 2 shows the swath coverage acquired in a region of the Arctic Ocean north of Alaska from Level 1B (L1B) data (left image) and the IST map product (right image). L1B is a swath (scene or granule) of MODIS data geolocated to latitude and longitude centers of 1-km resolution pixels and is available in each of the 36 bands. The MODIS L1B image (left) is shown as a composite of MODIS bands 1 (0.62–0.67 μm), 4 (0.545–0.565 μm), and 3 (0.459–0.479 μm). The MODIS IST map (right) also shows ice extent because any pixel that has a temperature of less than 271.5 K is considered to be ice, and any pixel with a temperature of 271.5 K or greater is considered to be open water. Because sea ice is saline, it freezes at a temperature that is less than 273.15 K (the freezing point of fresh water); we use 271.5 K as the cutoff temperature between water and ice for the "cold-period" images in the Arctic Basin, although a user can select their own cutoff temperature based on the IST to develop a sea ice extent map. During the "warm period" in the summer months, melting snow and meltponds

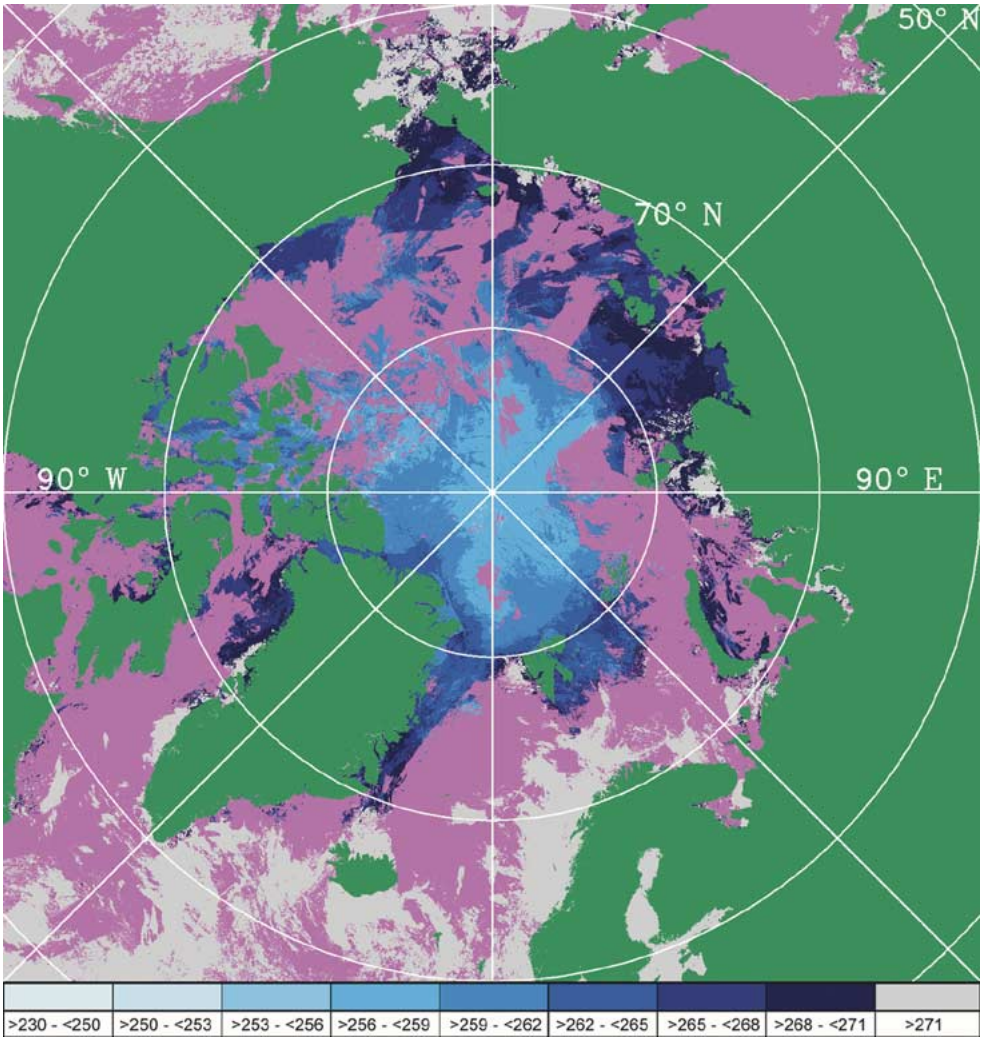

Fig. 1. Prototype (average of May 15–19, 2000) of the future eight-day composite sea ice surface temperature (IST) global EASE-Grid composite product of the north polar area MOD29C2 (prototype utilizes only five days of data). Color key shows ISTs from 230–271 K. The color scale represents IST in Kelvin. Clouds are shown in pink. In the compositing algorithm, sea ice in each cell has to be mapped for two or more days in a row; otherwise, it will be shown as a cloud. This reduces the errors of commission in the composited product.

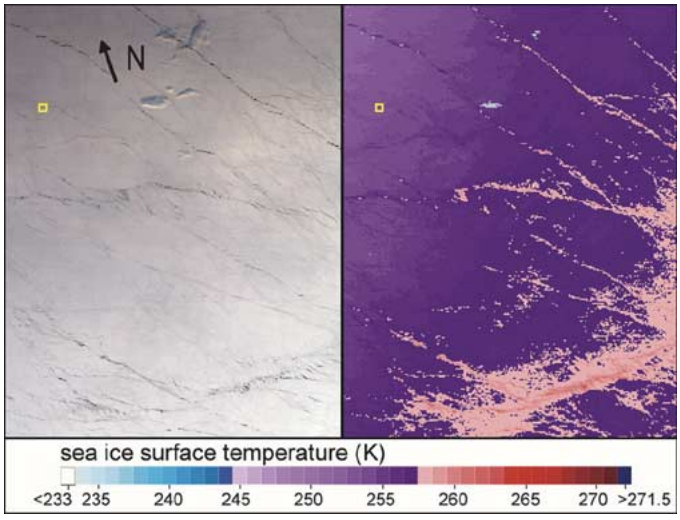

Fig. 2. (Left) True-color Terra MODIS image using bands 1 (0.62–0.67 μm), 4 (0.545–0.565 μm), and 3 (0.459–0.479 μm) derived from Terra MODIS Level 1B data, March 6, 2003 (22:45 UTC), in the Arctic Ocean north of Alaska. (right) Terra MODIS ice surface temperature map product of the same area at the same date and time. The location of the J-CAD 5 drifting buoy is shown inside the small yellow box at 76.91° N, 162.50° W (upper left). The color scale represents IST in Kelvin.

will likely have temperatures nearer that of melting fresh water ice (273.15 K) because meltwater on the surface of multiyear floes is less saline than water on top of first-year floes, since salts are ejected when an ice floe survives long enough to become a multiyear floe.

There are several different data product levels starting with Level 2 (L2). An L2 product is a geophysical product that remains in latitude and longitude orientation; it has not been temporally or spatially manipulated. A level-2G (L2G) product is a gridded format of a map projection. The L2G data are comprised of tiles, each tile being a piece, e.g., 10° latitude by 10° longitude area, of a map projection. Level-2 data products are gridded into L2G tiles by mapping the L2 pixels into cells of a tile in the map projection grid. The L2G algorithm creates a gridded product necessary for development of the level-3 (L3) products. An L3 product is a geophysical product that has been temporally and or spatially manipulated and, for sea ice, is gridded into the final product, also an L3 product, a daily global sea ice product for the north and south polar areas in the EASE-Grid projection at ∼4-km resolution (Fig. 1).

Both the Terra and Aqua MODIS products may be ordered through the NSIDC Distributed Active Archive Center (DAAC)

Earth Observing System (EOS) Data Gateway (EDG) at http://nsidc.org/~imswww/pub/imswelcome/index.html [40]. MOD29 is the Earth Science Data Type (ESDT) of the MODIS sea ice products for Terra, and MYD29 is the ESDT for Aqua. Terra "Collection 4" or Version 4 represents the most advanced algorithms, and the products in Terra Collection 4 are improved relative to earlier collections. When Terra Collection 5 begins in 2004, all the data will be reprocessed beginning February 24, 2000 (the date of "first light" of the Terra MODIS instrument, following the December 18, 1999, Terra launch) and, continuing to the present, into a consistent dataset. Similarly, the most advanced algorithms for Aqua are Version 3. Aqua Collection 4 reprocessing began in January of 2004, and all of the data will be reprocessed beginning June 24, 2002 (the date of "first light" of the Aqua MODIS instrument following the May 4, 2002, Aqua launch), and continuing to the present.

The content of the sea ice data products differs between day (MOD29P1D or MYD29P1D) and night (MOD29P1N or MYD29P1N) because MODIS visible data are not acquired when the sensor is in night mode and because the cloud mask for the nighttime IST product is different from the daytime cloud mask [39]. The day product (MOD29P1D or MYD29P1D) contains sea ice extent by reflectance and by IST, while the night product (MOD29P1N or MYD29P1N) contains only IST data processed from MODIS thermal data acquired during the night mode operation of the sensor [35]. These designations (Table I) should be used when ordering MODIS data from NSIDC.

A. Sea Ice Surface Temperature

The IST algorithm is the same for both the Terra and Aqua MODIS instruments. The split-window technique is implemented as a simple regression model of the form

$$T_s = a + bT_{11} + c(T_{11} - T_{12}) + d[(T_{11} - T_{12})(\sec\theta - 1)] \quad (1)$$

where T_s is the surface temperature, T_{11} and T_{12} are the satellite measured brightness temperatures in the 11 and 12 μm channels (MODIS channels 31 and 32), θ is the sensor scan angle, and a, b, c, and d are regression coefficients. The split-window temperature difference is proportional to the atmospheric water vapor amount, and the scan angle provides information on the path length.

To determine the empirical relationship in (1), radiosonde data from drifting ice- and land-based stations were used with a radiative transfer model LOWTRAN [41] to simulate the sensor brightness temperatures or skin temperatures with atmospheric profiles used to define atmospheric contributions. The sensor spectral response functions were convolved with the calculated radiances and converted to brightness temperatures for each radiosonde profile. The surface temperatures used in the model calculations were then regressed against the simulated brightness temperatures to determine the coefficients. Radiosonde data poleward of 65° latitude were taken from three archives: the North Pole archive, the National Center for Atmospheric Research (NCAR) archive, and the Historical Arctic Rawinsonde archive [42]. Profile data for Antarctica are from the Antarctic Radiosonde Data Set [43], a compilation of data from 18 land stations, including 16 coastal stations and two interior stations. More than 1000 profiles were used in the each of the Arctic and Antarctic analyses. The spectral scan-angle-dependent emissivities of snow as specified in [17] were used in the radiative transfer calculations. The regression coefficients in (1) were determined separately for the Arctic and Antarctic and for three temperature ranges.

Correlations between estimated and actual surface temperatures in the regression analysis are greater than 0.97 in all cases. RMS errors range from less than 0.1–0.3 K, with the larger values corresponding to higher temperatures. This is the same as for the AVHRR results presented in [17].

For temperatures above the melting point, a mixture of snow/ice and melt ponds is assumed. The emissivity is a weighted sum of snow and fresh-water emissivities, where the weights are 0.8 for snow and 0.2 for water. This is only an approximation, however, as the area fraction of snow and melt ponds can be very different from these values [17].

Atmospheric effects that result from melt ponds are taken into account to some extent in that the algorithm coefficients are based on a broad range of temperature and, hence humidity conditions. Of course, not all the temperature/humidity profiles with surface temperatures near the melting point will have the same humidity. But the effect will be small, on the order of 0.1–0.3 K, as indicated in the RMS error values of the estimated versus actual surface temperatures that come from the regression used in deriving the coefficients. In other words, the variability in humidity that results from mixing melt ponds and pack ice in the same pixel should not be any larger than the variability in the radiosonde profiles used in developing the coefficients, which yield RMS error differences of 0.1–0.3 K.

For the AVHRR, some sea surface temperature methods also employ the 3.7-μm channel. The use of this channel would be limited to nighttime analyses because it measures emitted thermal energy as well as reflected solar radiation. However, this channel is of low precision and often noisy at low temperatures when the amount of emitted energy is small, typical of the polar night. For the AVHRR, it was found that the inclusion of the 3.7-μm channel in (1) reduced the regression RMS error by only 0.003 K, which we do not consider a significant improvement in accuracy. Nevertheless, both the 3.7- and 3.9-μm MODIS channels (channels 20 and 21) will be investigated further in the future to determine if their use will improve the MODIS-derived IST.

Fig. 3 shows a MODIS IST map of sea ice in the northern Greenland Sea. Note the lower ISTs in this map as compared to those in the Arctic Ocean north of Alaska (Fig. 2). The climatological surface air temperature is colder by more than 10 K north of Greenland as compared to the Arctic Ocean just north of Alaska (see data in [12]). In both scenes, the recently refrozen leads are obvious as evidenced by their higher relative temperatures. Areas having higher relative temperatures may correspond with thinner ice; IST can often be used to detect new and young ice [44]. Well-developed ice floes are evident in the Greenland Sea (Fig. 3) because this is an active area and near the ice edge, while the area north of Alaska (Fig. 2) is a much

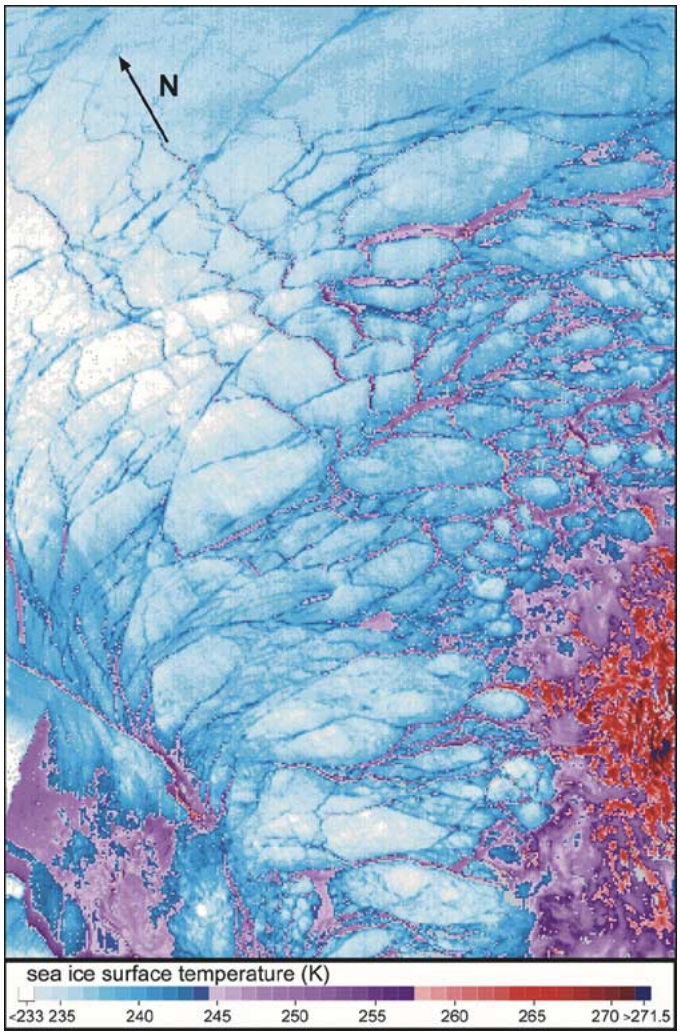

Fig. 3. Terra MODIS ice surface temperature (IST) product (MOD29) acquired on March 12, 2003 (18:45 UTC), in the northern Greenland Sea in the Arctic Ocean. The approximate center point of the image is 81.7° N, 1.0° E. The color scale represents IST in Kelvin.

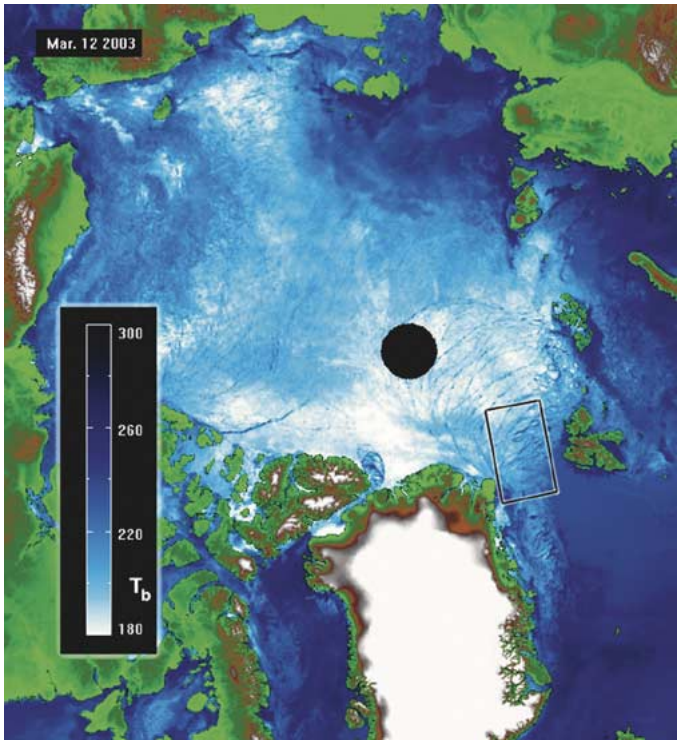

Fig. 4. AMSR-E 89-GHz vertically polarized image from the Aqua satellite, averaged from several swaths of data acquired on March 12, 2003, at a spatial resolution of ∼5 km. The rectangular box east–northeast of Greenland is the area of the MODIS IST image from Fig. 3. Microwave brightness temperatures from 180–300 K are shown in the scale.

more stable area, and thus, the ice has not been broken apart into distinct floes.

Note the area of the highest ISTs in Fig. 3, shown in the various shades of red in the southeastern part of the scene. This corresponds to an area of "warmer ice" or of very low ice concentration approaching the ice edge. Open water (with an IST exceeding 271.5 K) is also visible there. Though the ice edge cannot be seen on the full swath of the MODIS IST product due to obscuration by cloudcover, it is evident on an 89-GHz vertically polarized Advanced Microwave Scanning Radiometer-EOS (AMSR-E) image shown in Fig. 4. The location of the MODIS image (Fig. 3) is shown in the box east–northeast of Greenland in Fig. 4. The scale represents microwave brightness temperatures (T_B) from 180–300 K. Note that there is a general trend toward lower T_B's (Fig. 4) and lower ISTs (Fig. 3) toward the northwest in the rectangular study area. An algorithm to derive near-surface ice temperature (not IST) using AMSR data has been developed [10] and will be validated using data from recently completed and planned field campaigns [45]. For first-year floes, the AMSR-derived temperature is basically that of the snow/ice interface because the snow cover under dry conditions is transparent to the radiation emanating from the first-year ice, whereas for multiyear floes, the temperature represents a weighted-average of the freeboard portion of the ice [7], [8], [10].

Previous work has also shown that the quality of ice temperature retrievals from the SSM/I improves if the atmospheric attenuation is accounted for [46]. Furthermore, the ice physical temperature (not IST) trends from the SSM/I generally agree with those recorded by *in situ* buoys and that the ice temperatures are warmer than the buoy temperatures. This is expected because the buoy data represent local air temperatures, whereas the brightness temperatures originate at the warmer snow–ice interface.

B. Land and Cloud Masking in the Data Products

Land is masked using the 1-km resolution United States Geological Survey (USGS) global land/water mask [47] stored in the MODIS geolocation product [37]. The land/water mask is used by both the sea ice algorithm and cloud-masking algorithm to determine if a pixel is land or ocean for processing in the algorithms. An issue with this land/water mask is that ice shelves, such as the Ross Ice Shelf of Antarctica, are classified as land and not as part of the ocean because they emanate from the ice sheet. Consequently, ice shelves have not been included in the MODIS sea ice products. Improved coastline data that includes ice shelves as ocean have been developed and will be integrated into a future improved land/water mask. The new land/water mask will be implemented in Aqua Collection 4 and Terra Collection 5, in 2004. Following its implementation, it will be pos-

sible to monitor the movements of large icebergs that calve from the ice shelves in Antarctica on the sea ice maps.

Many situations occur that make it very difficult to identify clouds over sea ice in the daytime or nighttime even with the many visible, near-infrared, and infrared MODIS bands. If the MODIS cloud mask reports a "certain cloud" condition for a pixel, then the sea ice product is reported as cloud for that same pixel [39]. If the cloud mask reports that the observation is "probably clear," or "confident clear," then it is interpreted as clear, and the sea ice algorithm analyzes the pixel for IST.

The accuracy of the MODIS cloud mask over snow and ice varies, with the highest accuracy generally found for daytime data and the lowest accuracy in darkness. Low illumination and the similar reflectance characteristics of clouds and sea ice at visible wavelengths cause difficulties in cloud masking using MODIS data. Additionally, atmospheric inversions can cause surface temperatures to be colder than the temperature of some clouds [48]. Snow/cloud discrimination problems are exacerbated during the polar night because the MODIS reflective bands are not useful during darkness. The absolute accuracy of the MODIS cloud mask used in the sea ice algorithm is not known.

Ice-crystal precipitation (ICP) plays a role in IST retrieval. A previous study has shown that if ICP has an optical depth of 0.34 (and was not detected as a cloud), the error in IST would be $\sim$4 K [16]. However, the study concluded that ICP with an optical depth of $>$0.3 would probably be detected as a cloud and, therefore, not be a problem for IST retrieval [16]. Optically thinner ICP would present a problem. This is an issue with the MODIS cloud mask procedure [39] and, therefore, cannot be addressed in detail in this paper.

The Aqua MODIS cloud mask algorithm was revised to use band 7 (2.1 μm) in place of band 6 (1.6 μm) because most of the detectors on the Aqua MODIS in band 6 are nonfunctional. The revised Aqua cloud mask algorithm has been in operation since May 20, 2003.

A particular problem for mapping clouds over sea ice is the identification of thin clouds and fog. Fog often develops over sea-ice-covered waters when water vapor forms following the formation of leads and polynyas. While it may be possible to see the sea ice on a MODIS image, and even map the sea ice through the fog, it is not possible to retrieve an accurate IST through fog.

IV. IST Validation

In order to determine the accuracy of the MODIS IST algorithm, MODIS-derived skin temperature and the observed surface air temperature at the South Pole station were compared (Fig. 5). (Skin temperature data at the South Pole were not available.) Though a land site, the South Pole is a good study site because surface-based cloud measurements are available. The results represent 255 cases and are primarily nighttime cases, from April–December 2001. Scenes were identified as clear by examining micropulse lidar data at the South Pole station. The closest pixel was used, i.e., no averaging of adjacent pixels was done. The variability in the two measurements is greatest for low surface temperatures, possibly due to the lower radiometric

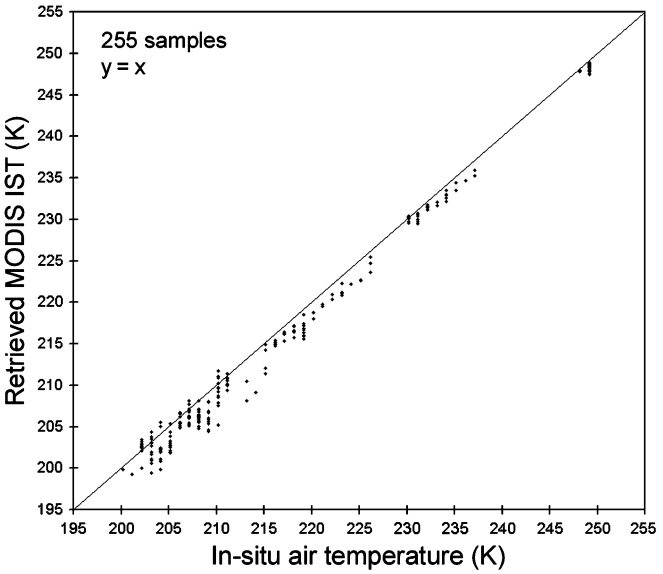

Fig. 5. MODIS IST-retrieved temperatures and measured surface temperatures at the South Pole station in Antarctica. Results are from a comparison of MODIS-derived skin temperature and the observed *in situ* surface air temperature at the South Pole, primarily nighttime cases for the period April–December 2001. Scenes were identified as clear by examining micropulse lidar data at South Pole station.

accuracy of the MODIS infrared channels at such extreme temperatures. There is a bias of -1.2 K and an RMS error of 1.7 K, where the negative bias means that the satellite-derived skin temperature is, on average, lower than the measured surface air temperature. This difference is almost certainly due to the skin and air temperature differences that are common in the presence of atmospheric temperature inversions. If we recalculate the RMS error after subtracting the bias from each value, the adjusted RMS error is 1.2 K.

Validation in the Arctic Ocean was also conducted using meteorological data from the Prudhoe Bay and Nome tide stations, as well as from drifting buoys. Data from the NOAA National Ocean Service (NOS) Center for Operational Oceanographic Products and Service (NOAA/NOS CO-OPS) program (http://www.co-ops.nos.noaa.gov/co-ops.html) meteorological station located at the Prudhoe Bay (70° 24.0′ N, 148° 31.6′ W), and Nome (64° 30′ N, 165° 25.8′ W) Alaska tide stations were studied. Air temperatures from drifting buoys were also used to validate the Terra and Aqua MODIS IST maps. The North Pole Environmental Observatory (NPEO) provides long-term measurements that are needed to track changes in the Arctic environment, including an automated drifting station consisting of clusters of buoys fixed to the drifting sea ice [49]. The buoys, tracked with global-positioning system receivers, measure atmospheric, ice, and other geophysical quantities in the Arctic Ocean. Air temperature is acquired at a height of $\sim$1.2 m. The Japan Marine Science and Technology Center (JAMSTEC) Compact Arctic Drifter 1, or J-CAD 1, was the first in a series that began acquiring measurements in April 2000 in the Arctic Ocean. For validation of the MODIS IST, we used data from J-CADs 4 and 5.

The Prudhoe Bay tide station, established in July 1990, is located at the end of a causeway north of Prudhoe Bay. The air

temperature measurements are acquired at a height of ∼9 m above sea level [50]. The tide station also provides information on tides (water level) and barometric pressure, wind speed, direction, and gust, including hourly air and water temperature data. The closest MODIS pixel on the IST map was used to compare with the Prudhoe Bay air temperatures. (The geolocation is 37 m along-track and 43 m along-scan for Terra, and 45 m along-track, and 67 m along-scan for Aqua.) The nearest (in time) air temperature as provided by the NOAA/NOS CO-OPS program was used unless the MODIS data acquisition was on the half hour, and in those cases, the two closest hourly air temperatures were averaged.

Radionov *et al.* [51] show that in the Arctic Basin during the cold period (defined as October through May) when the cloud cover is continuous, the snow surface temperature did not differ from the air temperature measured at a height of 2 m. However, under cloud-free conditions, the difference reached 6–7 K, the snow temperature being sharply lower compared with the 2-m air temperature due to longwave radiative cooling when the sky was clear. During the Arctic cold period, the temperature of the snow (250 measurements per month) was lower by an average of 0.6 K than the 2-m air temperature for both cloudy and cloud-free conditions. During the warm period, defined as June through August, the average temperature of the snow was 0.7 K lower than the 2-m air temperature (125–246 measurements per month) [51]. Based on this information, a bias of at least −0.6 K should be considered when comparing air temperature measurements to the MODIS IST retrievals because radiative cooling for our dataset should be even greater than with Radionov's data, since all of our measurements were acquired under clear-sky conditions during the cold period, and the Radionov *et al.* data included all sky conditions.

Results from the SHEBA Experiment reveal even more information on the differences expected between skin and near-surface air temperatures. From October 1997 to October 1998, the SHEBA ice floe drifted more than 1400 km in the Beaufort and Chukchi Seas with the latitude varying from 74°N to 81°N. A 20-m high instrumented tower was located on the floe. The differences between the skin temperature and the 8-m air temperature averaged ∼ 1.75 °C between November and February, and ∼ 0.75 °C in March and April, and ∼ 0 °C in May. These are average values, as the actual differences depend on wind and cloud cover conditions [52], [53]. During cold episodes, the daily surface temperatures at SHEBA could be as much as 5 °C lower than at the 10-m level [52].

Fig. 6 shows a comparison of the meteorological station or buoy air temperatures and the MODIS-derived ISTs using 25 scenes that were deemed to be free of clouds and fog at the measurement sites by visual inspection of the MODIS data. This dataset reveals a bias of −0.9 K and an RMS error of 1.6 K. If we adjust the air temperatures derived from the co-op station and the drifting buoys by subtracting the bias from each value, then the recalculated RMS error is 1.3 K.

Table II summarizes the comparison of the MODIS-derived ISTs with the Alaska tide stations and the Arctic drifting buoy temperatures. Also shown are the times that each measurement was acquired and the wind speeds (when available).

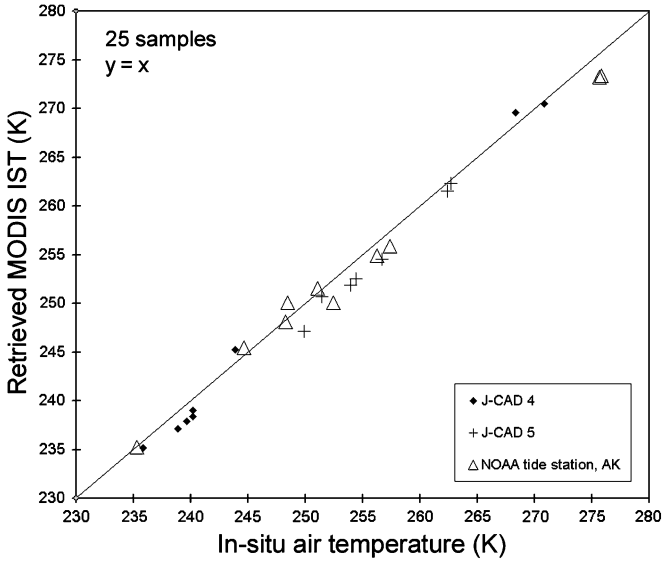

Fig. 6. MODIS IST-retrieved skin temperatures and measured surface temperatures in three different areas of the Arctic Ocean on various dates between January 25, 2002, and May 9, 2003. The MODIS pixels were visually screened for the likely presence of cloud or fog, and this dataset represents a subset of the dataset shown in Fig. 7. The *in situ* temperatures were acquired from the Japan Marine Science and Technology Center (JAMSTEC) Compact Arctic Drifter 4 and 5, or J-CAD 4 and J-CAD 5 buoys, and from the tide station at Prudhoe Bay, AK (see Table II and text for explanation).

Initially, 54 cases were selected based on the MODIS pixels being cloud-free according to the MODIS cloud mask. These cases consisted of meteorological station or buoy air temperatures and nearly coincident (temporally) MODIS ISTs (see Table II). Of these cases, 29 were rejected, based on close visual inspection of the accompanying MODIS L1B images or the MODIS sea ice maps (when darkness precluded the use of the L1B data), which revealed the likely presence of clouds or fog, and the remaining 25 cases were used to develop the graph in Fig. 6. Fig. 7 shows the results using all 54 data points, revealing a bias of −2.1 K and an RMSE of 3.7 K. With the bias removed from each value, the RMS error is 3.0 K.

The difference between the *in situ* air temperatures and the MODIS ISTs is slightly greater, on average, when wind speeds are lower, as would be expected; however, the relationship is very weak. As the wind speed increases, there is more mixing in the lower atmosphere; thus, there is less likely to be an inversion with a strong temperature gradient. The wind speeds reported for J-CAD 5 can explain some of the difference between air temperature and the MODIS IST (Table II).

V. Limitations

Though the MODIS-derived IST algorithm performs extremely well under totally clear-sky conditions, with an accuracy (RMS error) of 1.2–1.3 K, polar weather is often a factor that precludes accurate IST retrieval using MODIS data. It is virtually impossible to determine whether conditions are completely cloud free when deriving IST in an automated way using the MODIS cloud mask algorithm summary result called "certain cloud." That summary result is based on several cloud tests applied in the cloud mask and confidences associated with the tests. In some situations, the tests can fail to detect clouds or may detect clouds falsely, resulting in an inaccurate result. The

TABLE II
IST VALIDATION SUMMARY FOR J-CAD 4 AND 5 DRIFTING BUOYS, AND THE NOME AND PRUDHOE BAY, ALASKA, TIDE STATIONS. "TERRA" AND "AQUA" REFER TO IMAGES ACQUIRED FROM EITHER THE TERRA OR AQUA MODIS INSTRUMENTS, AND 003 AND 004 REFER TO EITHER VERSION 3 OR 4 OF THE MODIS IST ALGORITHM. ALL TERRA DATA ARE VERSION 4 AND ALL AQUA DATA ARE VERSION 3; THE TERRA VERSION 4 ALGORITHM IS THE SAME AS THE AQUA VERSION 3 ALGORITHM. BUOY OR STATION TEMPERATURES ARE SUBTRACTED FROM THE MODIS ISTs TO DERIVE THE DIFFERENCE. THE 25 CASES THAT WERE USED IN FIG. 5, WHERE VISUAL CLOUD SCREENING WAS DONE, ARE SHOWN WITH AN ASTERISK. †INDICATES NOME, AK TIDE STATION. ALL OTHER TIDE STATIONS ARE PRUDHOE BAY, AK

J-CAD 4 – JAMSTEC buoy

Date	Time (UTC) – data specification	MODIS IST K	J-CAD 4 buoy K	Difference K	Wind speed (m/s)
Mar 1 2003*	1905 – Terra 004	235.1	235.9	-0.8	n/a
Mar 2 2003	0345 – Aqua 003	236.6	238.2	-1.6	n/a
Mar 2 2003	0840 – Aqua 003	241.8	240.9	0.9	n/a
Mar 2 2003	1315 – Terra 004	245.8	242.4	3.4	n/a
Mar 2 2003*	1810 – Terra 004	239.0	240.2	-1.2	n/a
Mar 3 2003*	0250 – Aqua 003	237.1	238.9	-1.8	n/a
Mar 3 2003*	0745 – Aqua 003	237.9	239.7	-1.8	n/a
Mar 3 2003*	1100 – Aqua 003	238.4	240.2	-1.8	n/a
Mar 4 2003	0650 – Aqua 003	239.2	246.9	-7.7	n/a
Mar 5 2003	0555 – Aqua 003	237.3	242.4	-5.1	n/a
Mar 9 2003*	1500 – Terra 004	245.3	243.9	1.4	n/a
Mar 10 2003	1405 – Terra 004	237.5	236.9	0.6	n/a
Mar 10 2003	1720 – Terra 004	237.8	236.4	1.4	n/a
Mar 12 2003	1215 – Terra 004	243.9	243.2	0.7	n/a
Mar 12 2003	1530 – Terra 004	241.8	245.3	-3.5	n/a
Mar 13 2003	1435 – Terra 004	248.4	246.5	1.9	n/a
Mar 13 2003	1750 – Terra 004	242.8	243.9	-1.1	n/a
Mar 18 2003	1315 – Terra 004	252.3	248.7	3.6	n/a
Apr 14 2003*	2105 – Terra 004	269.6	268.4	1.2	n/a
Apr 15 2003*	2010 – Terra 004	270.5	270.9	-0.4	n/a

J-CAD 5 – JAMSTEC buoy

Date	Time (UTC) – data specification	MODIS IST K	J-CAD 5 buoy K	Difference K	Wind speed (m/s)
Mar 5 2003	0350 – Terra 004	245.0	253.4	-8.4	4.50
Mar 5 2003	1905 – Aqua 003	242.4	246.2	-3.8	2.00
Mar 6 2003	1810 – Aqua 003	256.6	260.4	-3.8	5.25
Mar 6 2003*	2245 – Terra 004	254.6	256.7	-2.1	6.00
Mar 7 2003*	0200 – Terra 004	252.5	254.4	-1.9	7.00
Mar 19 2003	0540 – Terra 004	235.8	242.4	-6.6	0.50
Mar 20 2003	0445 – Terra 004	237.9	245.2	-7.3	1.50
Mar 21 2003	0350 – Terra 004	239.4	250.4	-11.0	1.00
Mar 28 2003	0535 – Terra 004	248.8	252.7	-3.9	3.00
Mar 29 2003	0440 – Terra 004	247.8	251.4	-3.6	3.50
Mar 29 2003*	0755 – Terra 004	247.1	249.9	-2.8	4.00
Mar 31 2003	0605 – Terra 004	245.0	249.2	-4.2	n/a
Apr 16 2003*	0250 – Terra 004	251.9	253.9	-2.0	5.25
Apr 16 2003*	2240 – Terra 004	250.7	251.4	-0.7	3.00
May 8 2003*	2340 – Terra 004	262.3	262.7	-0.4	3.50
May 9 2003*	0255 – Terra 004	261.5	262.4	-0.9	4.00

cloud mask that is provided for use with MODIS products [39], [54] provides a conservative estimate of cloud cover but often does not map thin fog as a cloud. The cloud mask also provides individual spectral tests that a sophisticated user can employ separately (or together) to develop a cloud mask that is more specific to their particular study area. Improved cloud masking results have been attained in the MODIS snow algorithm [55] when selected spectral tests from the MODIS cloud mask are used to create a cloud mask specific to snow-covered land surfaces, but has not yet been attempted for the MODIS sea ice products.

VI. DISCUSSION AND CONCLUSION

The 1-km MODIS IST product currently represents the only daily global IST product available at such a fine resolution and may be used in energy-balance modeling. The clear-sky limitation can possibly be obviated in the future using passive-microwave data in conjunction with MODIS data. Passive-microwave-derived ice temperatures are not directly comparable with ISTs because the passive-microwave temperature is an integrated measure of the temperature of the upper layers of the sea ice or/and overlying snow cover, and the depth from which the microwave energy emanates depends on the emissivity of the snow/ice. Maslanik and Key [29] developed a technique to combine AVHRR-derived ISTs with SSM/I data to derive IST. Though their temperatures appeared reasonable when compared with climatological averages, the absolute accuracy of the derived temperatures could not be determined.

However, following from prior work (e.g., [10] and [29]), if a relationship can be determined between MODIS-derived

TABLE II
(Continued.) IST VALIDATION SUMMARY FOR J-CAD 4 AND 5 DRIFTING BUOYS, AND THE NOME AND PRUDHOE BAY, ALASKA, TIDE STATIONS. "TERRA" AND "AQUA" REFER TO IMAGES ACQUIRED FROM EITHER THE TERRA OR AQUA MODIS INSTRUMENTS, AND 003 AND 004 REFER TO EITHER VERSION 3 OR 4 OF THE MODIS IST ALGORITHM. ALL TERRA DATA ARE VERSION 4 AND ALL AQUA DATA ARE VERSION 3; THE TERRA VERSION 4 ALGORITHM IS THE SAME AS THE AQUA VERSION 3 ALGORITHM. BUOY OR STATION TEMPERATURES ARE SUBTRACTED FROM THE MODIS ISTs TO DERIVE THE DIFFERENCE. THE 25 CASES THAT WERE USED IN FIG. 5, WHERE VISUAL CLOUD SCREENING WAS DONE, ARE SHOWN WITH AN ASTERISK. †INDICATES NOME, AK TIDE STATION. ALL OTHER TIDE STATIONS ARE PRUDHOE BAY, AK NOAA tide stations

Date	Time (UTC) – data specification	MODIS IST K	Prudhoe Bay K	Difference K	Wind speed (m/s)
Jan 22 2002	2200 – Terra 004	241.4	242.7	-1.3	0.0
Jan 25 2002*	2230 – Terra 004	235.3	235.3	0.0	0.0
Feb 27 2002	2135 – Terra 004	253.5	254.5	-1.0	9.9
Mar 3 2002*	2110 – Terra 004	245.5	244.7	0.8	5.8
Mar 29 2002*	2145 – Terra 004	248.1	248.3	-0.2	5.1
Mar 30 2002*	2230 – Terra 004	250.0	248.5	1.5	5.8
Mar 31 2002*	2135 – Terra 004	251.6	251.1	0.5	8.1
Apr 22 2002	0735 – Terra 004	246.1	255.1	-9.0	5.6
Apr 22 2002 †	0735 – Terra 004	254.4	258.9	-4.5	5.6
May 21 2002*	2205 – Terra 004	273.2	275.7	-2.5	5.9
May 22 2002*	2110 – Terra 004	273.4	275.9	-2.5	7.0
Nov 20 2002 *	2210 – Terra 004	250.1	252.5	-2.4	14.4
Nov 20 2002	2350 – Terra 004	249.1	252.1	-3.0	13.7
Jan 19 2003 *	2055 – Terra 004	254.9	256.3	-1.4	17.9
Jan 19 2003 *	2235 – Terra 004	255.9	257.4	-1.5	19.7
Jan 19 2003 †	2235 – Terra 004	266.3	272.6	-6.3	1.8
Jan 20 2003	0640 – Terra 004	256.4	258.4	-2.0	16.9
Jan 20 2003	2140 – Terra 004	255.6	258.9	-3.3	8.4

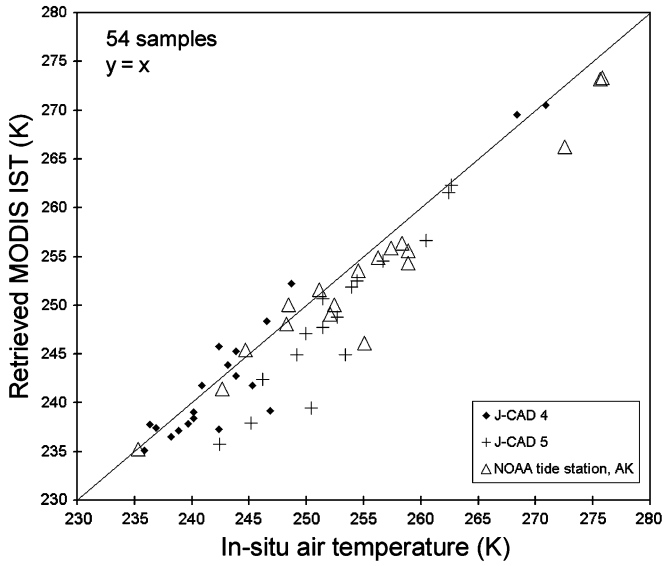

Fig. 7. MODIS IST-retrieved skin temperatures and measured surface temperatures in three different areas of the Arctic Ocean on various dates between January 22, 2002, and May 9, 2003. These cases were derived from cloud-free parts of the MODIS IST product, by utilizing the standard MODIS cloud mask to detect clouds. The cases plotted in Fig. 6 are contained within this dataset. The *in situ* temperatures were acquired from the Japan Marine Science and Technology Center (JAMSTEC) Compact Arctic Drifter 4 and 5, or J-CAD 4 and J-CAD 5 buoys, and the tide stations at Nome and Prudhoe Bay, AK (see Table II and text for explanation).

ISTs and AMSR-derived ice temperature, then the passive-microwave-derived ice temperatures can be used to approximate IST even through clouds. Such a product would provide modelers global IST data daily through cloud cover and darkness, though at a coarser resolution than is possible from MODIS alone.

With both the AMSR-E and the MODIS on the Aqua satellite, it is possible to assess the relationship between MODIS-derived IST and ice temperature derived from the AMSR-E. The recent launches of the AMSR sensors on the EOS Aqua and Advanced Earth Observing Satellite II spacecraft and the planned Defense Meteorological Satellite Program Special Sensor Microwave Imager/Sounder and the National Polar-orbiting Operational Environmental Satellite System missions will extend the sea ice records into the foreseeable future.

With regard to the "mixed-pixel problem," the presence of mixed pixels will not increase the overall error in ISTs significantly. The difference in surface emissivity for thin, bare ice or open water versus pack ice is small in the infrared part of the spectrum. So, the effect of the other surface types is that the surface temperature, and possibly the lower tropospheric humidity, will be higher. The IST algorithm is based on a wide range of temperature and humidity conditions, so this is taken into account to some extent. On the other hand, there can be a range of humidity conditions for a given surface temperature, even though these two parameters are physically tied together.

Additionally, thin ice near the buoy may cause the IST of the MODIS pixel to be unrepresentative. While a standard deviation of the ISTs of the adjacent pixel values would be good to determine, generally it is also possible to tell by looking at the ISTs of the nearby pixels that the ISTs are representative.

The MODIS sea ice products represent a suite of products that is useful as a component of a climate data record for sea ice extent and IST. Additional work will need to be done in order to validate the products in all seasons; however, the MODIS IST product appears to be of comparable or superior quality as compared to predecessor datasets, such as products derived from the AVHRR. (The Noise Equivalent Temperature differences for MODIS channels 31 and 32 and for the AVHRR infrafred channels were designed to be 0.05 and 0.12 K, respectively, at 300 K. Furthermore, the cloud masking with MODIS is an improvement over the cloud masking with the AVHRR.) Thus, the

MODIS-derived products should compare well with products that will be derived from future sensors for determination of sea ice extent and IST.

The MODIS-derived IST provides an excellent measurement of the actual temperature of the surface of the sea ice during the Arctic cold period. Using cloud-free data as determined using the MODIS standard cloud mask (which includes some pixels affected by fog), the bias is −2.1 K with an RMS error of 3.7 K, and with the bias removed, the RMS error or accuracy is 3.0 K. However, under clear-sky conditions, two different validation studies from the clear-sky cases at the South Pole and in the Arctic Ocean show excellent agreement, with a bias of −1.2 and −0.9 K and an uncertainty of 1.7 and 1.6 K, respectively. With the bias removed, the RMS error or accuracy for the South Pole and the Arctic Ocean is 1.2 and 1.3 K, respectively.

ACKNOWLEDGMENT

MODIS sea ice map products were obtained from the National Snow and Ice Data Center, Boulder, CO. The AMSR-E instrument was provided by Japan's National Space Development Agency.

The authors would like to thank Y. Liu (Cooperative Institute for Meteorological Satellite Studies, University of Wisconsin) for providing the South Pole IST plot; the North Pole Environmental Observatory for use of the drifting buoy data; and N. DiGirolamo and A. Ivanoff (SSAI, Inc.) for providing programming support. P. Guest (Naval Postgraduate School) provided useful information about the meteorological tower during the SHEBA experiment. The authors would also like to thank the three anonymous reviewers for very helpful comments.

REFERENCES

[1] D. J. Cavalieri, P. Gloersen, C. L. Parkinson, J. C. Comiso, and H. J. Zwally, "Observed asymmetry in global sea ice changes," *Science*, vol. 278, pp. 1104–1106, 1997.

[2] K. Y. Vinnikov, A. Robock, R. J. Stouffer, J. E. Walsh, C. L. Parkinson, D. J. Cavalieri, J. F. B. Mitchell, D. Garrett, and V. F. Zakharov, "Global warming and Northern Hemisphere sea ice extent," *Science*, vol. 286, pp. 1934–1937, 1999.

[3] C. L. Parkinson and D. J. Cavalieri, "A 21 year record of Arctic sea-ice extents and their regional, seasonal and monthly variability and trends," *Ann. Glaciol.*, vol. 34, pp. 441–446, 2002.

[4] H. J. Zwally, J. C. Comiso, C. L. Parkinson, D. J. Cavalieri, and P. Gloersen, "Variability of Antarctic sea ice 1979–1998," *J. Geophys. Res.*, vol. 107, no. C5, 2002. DOI: 10.1029/2000JC000733.

[5] D. J. Cavalieri, C. L. Parkinson, and K. Y. Vinnikov, "30-year satellite record reveals contrasting Arctic and Antarctic decadal sea ice variability," *Geophys. Res. Lett.*, vol. 30, no. 18, 1970. DOI: 10.1029/2003GL018031.

[6] J. C. Comiso, "Warming trends in the Arctic from clear sky satellite observations," *J. Climate*, vol. 16, pp. 3498–3510, 2003.

[7] D. J. Cavalieri, P. Gloersen, and W. J. Campbell, "Determination of sea ice parameters with the Nimbus-7 SMMR," *J. Geophys. Res.*, vol. 89, pp. 5355–5369, 1984.

[8] P. Gloersen, W. J. Campbell, D. J. Cavalieri, J. C. Comiso, C. L. Parkinson, and H. J. Zwally, "Arctic and Antarctic Sea Ice, 1978–1987: Satellite passive microwave observations and analysis," Nat. Aeronautics Space Admin., Washington, DC, Special Pub. 511, 1992.

[9] C. A. Shuman, R. B. Alley, S. Anandakrishnan, and C. R. Stearns, "An empirical technique for estimating near-surface air temperature trends in central Greenland from SSM/I brightness temperatures," *Remote Sens. Environ.*, vol. 51, pp. 245–252, 1995.

[10] J. C. Comiso, D. J. Cavalieri, and T. Markus, "Sea ice concentration, ice temperature, and snow depth using AMSR-E data," *IEEE Trans. Geosci. Remote Sensing*, vol. 41, pp. 243–252, Feb. 2003.

[11] H. J. Zwally, J. C. Comiso, C. L. Parkinson, W. J. Campbell, F. D. Carsey, and P. Gloersen, "Antarctic sea ice, 1973–1976: Satellite passive-microwave observations," GPO, Washington, DC, NASA SP-459, 1983.

[12] C. L. Parkinson, J. C. Comiso, H. J. Zwally, D. J. Cavalieri, P. Gloersen, and W. J. Campbell, "Arctic sea ice, 1973–1976: Satellite passive-microwave observations," GPO, Washington, DC, NASA SP-487, 1987.

[13] K. R. Dedrick, K. Partington, M. Van Woert, C. A. Bertoia, and D. Benner, "U.S. National/Naval Ice Center digital sea ice data and climatology," *Can. J. Remote Sens.*, vol. 27, no. 5, pp. 457–475, 2001.

[14] J. C. Comiso, "Surface temperatures in the polar regions from Nimbus 7 temperature humidity infrared radiometer," *J. Geophys. Res.*, vol. 99, no. C3, pp. 5181–5200, 1994.

[15] R. W. Lindsay and D. A. Rothrock, "Arctic sea ice surface temperature from AVHRR," *J. Climate*, vol. 7, no. 1, pp. 174–183, 1993.

[16] J. Key and M. Haefliger, "Arctic ice surface temperature retrieval from AVHRR thermal channels," *J. Geophys. Res.*, vol. 97, no. D5, pp. 5885–5893, 1992.

[17] J. Key, J. Collins, C. Fowler, and R. Stone, "High-latitude surface temperature estimates from thermal satellite data," *Remote Sens. Environ.*, vol. 61, pp. 302–309, 1997.

[18] J. C. Comiso, "Satellite-observed variability and trend in sea-ice extent, surface temperature, albedo and clouds in the Arctic," *Ann. Glaciol.*, vol. 33, pp. 457–473, 2001.

[19] X. Wang and J. Key, "Recent trends in Arctic surface, cloud, and radiation properties from space," *Science*, vol. 299, no. 5613, pp. 1725–1728, 2003.

[20] R. E. Moritz, J. A. Curry, N. Untersteiner, and A. S. Thorndike, "Prospectus: Surface heat budget of the Arctic Ocean," SHEBA Project Office, Polar Sci. Center, Appl. Phys. Lab., Univ. Washington, Seattle, WA, NFSF-ARCSS OAII Tech. Rep. 3, 1993.

[21] J. Key, J. A. Maslanik, T. Papakyriakou, M. C. Serreze, and A. J. Schweiger, "On the validation of satellite-derived sea ice surface temperature," *Arctic*, vol. 47, no. 3, pp. 280–287, 1994.

[22] J. Maslanik, J. Key, C. Fowler, T. Nyguyen, and X. Wang, "Spatial and temporal variability of surface and cloud properties from satellite data during FIRE-ACE," *J. Geophys. Res.*, vol. 106, no. D14, pp. 15 233–15 249, 2001.

[23] C. Fowler, J. Maslanik, T. Haran, T. Scambos, J. Key, and W. Emery, "AVHRR Polar Pathfinder Twice-Daily 5 Km EASE-Grid Composites," National Snow and Ice Data Center, Boulder, CO, 2000.

[24] W. Meier, J. A. Maslanik, J. Key, and C. Fowler, "Retrieval of Arctic surface conditions and cloud properties from AVHRR data: A time series for the Beaufort Sea," in *Proc. IGARSS*, vol. 1, Lincoln, NE, May 27–31, 1996, pp. 73–75.

[25] J. Maslanik, C. Fowler, J. Key, T. Scambos, T. Hutchinson, and W. Emery, "AVHRR-based polar pathfinder products for modeling applications," *Ann. Glaciol.*, vol. 25, pp. 388–392, 1997.

[26] C. P. Prabhakara, G. Dalu, and V. G. Kunde, "Estimation of sea surface temperature from remote sensing in the 11–13 μm window region," *J. Geophys. Res.*, vol. 79, no. 33, pp. 5039–5044, 1974.

[27] R. Massom and J. C. Comiso, "The classification of Arctic sea ice types and the determination of surface temperature using advanced very high resolution radiometer data," *J. Geophys. Res.*, vol. 99, no. C3, pp. 5201–5218, 1994.

[28] Y. Yu, D. A. Rothrock, and R. W. Lindsay, "Accuracy of sea ice temperature derived from the Advanced Very High Resolution Radiometer," *J. Geophys. Res.*, vol. 100, pp. 4525–4532, 1995.

[29] J. A. Maslanik and J. Key, "Comparison and integration of ice-pack temperatures derived from AVHRR and passive microwave imagery," *Ann. Glaciol.*, vol. 17, pp. 372–378, 1993.

[30] D. K. Hall, A. T. C. Chang, and J. L. Foster, "Seasonal and interannual observations and modeling of the snowpack on the Arctic coastal plain of Alaska using satellite data," in *Proc. AWRA Symp. Cold Regions Hydrology*, pp. 521–529.

[31] W. L. Barnes, T. S. Pagano, and V. V. Salomonson, "Prelaunch characteristics of the Moderate Resolution Imaging Spectroradiometer (MODIS) on EOS-AM1," *IEEE Trans. Geosci. Remote Sensing*, vol. 36, pp. 1088–1100, July 1998.

[32] D. K. Hall, G. A. Riggs, V. V. Salomonson, N. E. DiGirolamo, and K. J. Bayr, "MODIS snow-cover products," *Remote Sens. Environ.*, vol. 83, pp. 181–194, 2002.

[33] C. O. Justice *et al.*, "The Moderate Resolution Imaging Spectroradiometer (MODIS): Land remote sensing for global change research," *IEEE Trans. Geosci. Remote Sensing*, vol. 36, pp. 1228–1249, July 1998.

[34] R. L. Armstrong and M. J. Brodzik, "An earth-gridded SSM/I data set for cryospheric studies and global change monitoring," *Adv. Space Res.*, vol. 10, pp. 155–163, 1995.
[35] G. A. Riggs, D. K. Hall, and V. V. Salomonson. (2003) MODIS Sea Ice User's Guide. [Online] Available: http://modis-snow-ice.gsfc.nasa.gov/siugkc.html.
[36] G. A. Riggs, D. K. Hall, and S. A. Ackerman, "Sea ice extent and classification mapping with the Moderate Resolution Imaging Spectroradiometer airborne simulator," *Remote Sens. Environ.*, vol. 68, pp. 152–163, 1999.
[37] B. Guenther, X. Xiong, V. V. Salomonson, W. L. Barnes, and J. Young, "On-orbit performance of the Earth Observing System Moderate Resolution Imaging Spectroradiometer; First year of data," *Remote Sens. Environ.*, vol. 83, pp. 16–30, 2002.
[38] R. Wolfe, M. Nishihama, A. J. Fleig, J. A. Kuyper, D. P. Roy, J. C. Storey, and F. S. Patt, "Achieving sub-pixel geolocation accuracy in support of MODIS land science," *Remote Sens. Environ.*, vol. 83, pp. 31–49, 2002.
[39] S. A. Ackerman, K. I. Strabala, P. W. P. Menzel, R. A. Frey, C. C. Moeller, and L. E. Gumley, "Discriminating clear sky from clouds with MODIS," *J. Geophys. Res.*, vol. 103, no. D24, pp. 32 141–32 157, 1998.
[40] G. R. Scharfen, D. K. Hall, S. J. S. Khalsa, J. D. Wolfe, M. C. Marquis, G. A. Riggs, and B. McLean, "Accessing the MODIS snow and ice products at the NSIDC DAAC," in *Proc. IGARSS*, Honolulu, HI, July 23–28, 2000, pp. 2059–2061.
[41] F. X. Kneizys, E. P. Shettle, L. W. Abreu, J. H. Chetwynd, G. P. Anderson, W. O. Gallery, J. E. A. Selby, and S. A. Clough, "Users guide to LOWTRAN 7," Air Force Geophys. Lab., Hanscom Air Force Base, MA, Tech. Rep. AFGL-TR-88-0177 (NTIS AD A206773), 1988.
[42] M. C. Serreze, J. D. Kahl, and R. C. Schnell, "Low-level temperature inversions of the Eurasian Arctic and comparisons with Soviet drifting station data," *J. Climate*, vol. 5, no. 6, pp. 615–629, 1992.
[43] W. M. Connolley and J. C. King, "Atmospheric water vapor transport to Antarctica inferred from radiosondes," *Q. J. R. Meteorol. Soc.*, vol. 119, pp. 325–342, 1993.
[44] R. S. Stone and J. R. Key, "The detectability of Arctic leads using thermal imagery under varying atmospheric conditions," *J. Geophys. Res.*, vol. 98, no. C7, pp. 12 469–12 482, 1993.
[45] D. J. Cavalieri, J. Maslanik, T. Markus, J. Stroeve, M. Sturm, J. Heinrichs, E. Kim, A. J. Gasiewski, and J. C. Comiso, "EOS Aqua AMSR-E Arctic sea ice validation program," in *Proc. Int. Soc. Optical Engineering 3rd Int. Asia–Pacific Environmental Remote Sensing Atmosphere, Ocean, Environment, Space Conf. Microwave Remote Sensing of the Atmosphere and Environment III*, vol. 4894, Hangzhou, China, Oct. 23–27, 2002, pp. 413–424.
[46] K. Steffen, J. Key, D. J. Cavalieri, J. Comiso, P. Gloersen, K. S.K. St. Germain, and I. Rubenstein, "The estimation of geophysical parameters using passive microwave algorithms," in *Microwave Remote Sensing of Sea Ice*, F. Carsey, Ed. Washington, DC: AGU, 1992, American Geophysical Union Monograph 68, pp. 201–231.
[47] USGS, "Landsat 7 image assessment system geometric," USGS EROS Data Center, Sioux Falls, SD, Algorithm Theoretical Basis Doc. Ver. , J. C. Storey, Ed., 1997.
[48] T. J. McIntire and J. J. Simpson, "Arctic sea ice, cloud, water, and lead classification using neural networks and 1.6 μm data," *IEEE Trans. Geosci. Remote Sensing*, vol. 40, pp. 1956–1972, Sept. 2002.
[49] J. H. Morison, K. Aagaard, K. K. Falkner, K. Hatakeyama, R. Moritz, J. E. Overland, D. Perovich, K. Shimada, M. Steele, T. Takizawa, and R. Woodgate, "North Pole environmental observatory delivers early results," *EOS*, vol. 83, no. 33, pp. 357, and 360–361, 2002.
[50] M. J. McCray, private communication, 2003.
[51] V. F. Radionov, N. N. Bryazgin, and E. I. Alexandrov, "The snow cover of the Arctic Basin," Appl. Physics Lab., Univ. Washington, Seattle, Tech. Rep. APL-UW TR 9701, 1997.
[52] P. Guest, private communication, Sept. 2003.
[53] P. O. G. Persson, C. W. Fairall, E. L. Andreas, P. S. Guest, and D. K. Perovich, "Measurements near the atmospheric surface flux group tower at SHEBA: Near-surface conditions and surface energy budget," *J. Geophys. Res.*, vol. 107, no. C10, 2002. DOI: 10.1029/2000JC999705.
[54] S. Platnick, M. D. King, S. A. Ackerman, W. P. Menzel, B. A. Baum, J. C. Riédi, and R. A Frey, "The MODIS cloud products: Algorithms and examples from Terra," *IEEE Trans. Geosci. Remote Sensing*, vol. 41, pp. 459–473, Feb. 2003.
[55] G. A. Riggs and D. K. Hall, "Reduction of cloud obscuration in the MODIS snow data product," in *Proc. 6th Eastern Snow Conf.*, June 5–7, 2003.

Dorothy K. Hall (M'03–SM'03) received the Ph.D. degree in geography from the University of Maryland, College Park, in 1980.

She has been with the NASA Goddard Space Flight Center (GSFC), Greenbelt, MD, since 1975. She is currently a Senior Research Scientist in the Hydrological Sciences Branch of the Laboratory for Hydrospheric Processes, GSFC. Her research interests include the remote sensing of snow, glacier, river, lake ice, and sea ice. She has been an investigator on various snow and ice projects using Landsat and synthetic aperture radar, as well as on science education projects, and is an Earth Observing System (EOS) Moderate Resolution Imaging Spectroradiometer (MODIS) Team Member. She was a Distinguished Visiting Scholar in the Department of Geography, University of Delaware in 2002.

Dr. Hall is a member and Past President of the Eastern Snow Conference, a member of the International Glaciological Society, and a member of the American Geophysical Union.

Jeffrey R. Key received the B.S. and M.S. degrees in environmental conservation from Northern Michigan University, Marquette, in 1977 and 1982, respectively, and the Ph.D. degree in climatology from the University of Colorado, Boulder, in 1988.

Since 1999, he has been a member of the Advanced Satellite Products Team, NOAA/NESDIS, Madison, WI, where his goal is to improve high-latitude snow, ice, and atmospheric satellite products and foster their use in numerical weather prediction systems. His research interests include the radiative effect of clouds on the surface energy budget, polar meteorology, satellite remote sensing of cloud and surface properties, and climate change.

Kimberly A. Casey received the A.B. degree in environmental chemistry from Washington University, St. Louis, MO, and is currently pursuing the M.S. degree at The Johns Hopkins University, Baltimore, MD.

She is currently a Scientific Analyst/Programmer with Science Systems and Applications, Inc., Greenbelt, MD. She is involved in the analysis and validation of MODIS snow and sea ice data products.

Ms. Casey is a member of the America Geophysical Union.

George A. Riggs received the B.S. degree from Nebraska Wesleyan University, Lincoln, in 1979, the M.S. degree from the University of Nebraska, Lincoln, in 1985, and the Ph.D. degree from the University of Montana, Missoula, in 1989.

He is currently a Senior Scientist with Science Systems and Applications, Inc., Greenbelt, MD. He is working with the MODIS snow and sea ice algorithm investigators developing the snow and sea ice algorithms. His responsibilities include algorithm development, testing, evaluation, and validation of the snow and sea ice data products generated for the Earth Observing System (EOS). His research interests include remote sensing of snow and sea ice, production of geophysical parameters for modeling, and global monitoring of the cyrosphere.

Donald J. Cavalieri received the B.S. degree in physics from the City College of New York in 1960, the M.A. degree in physics from Queens College of New York in 1967, and the Ph.D. degree in meteorology and oceanography from New York University in 1974.

He is currently a Senior Research Scientist in the Oceans and Ice Branch of the Laboratory for Hydrospheric Processes, Goddard Space Flight Center (GSFC), Greenbelt, MD. His research interests currently center on polar ocean processes and the microwave remote sensing of the cryosphere.

Dr. Cavalieri is a member of the American Geophysical Union and the American Meteorological Society.